

Electronic Supplementary Information

Electrospun manganese-cobalt oxide hollow nanofibres synthesized via combustion reactions and their lithium storage performance

Soo Min Hwang,^{‡§^a} So Yeun Kim,^{‡^{bc}} Jae-Geun Kim,^b Ki Jae Kim,^b Jong-Won Lee,^d Min-Sik Park,^{*b} Young-Jun Kim,^b Mohammed Shahabuddin,^e Yusuke Yamauchi^f and Jung Ho Kim,^{*a}

^a*Institute for Superconducting and Electronic Materials, University of Wollongong, North Wollongong, NSW 2500, Australia*

^b*Advanced Batteries Research Center, Korea Electronics Technology Institute, Seongnam-si, Gyeonggi-do 463-816, Republic of Korea*

^c*Department of Advanced Chemicals & Engineering, Chonnam National University, Gwangju 500-757, Republic of Korea*

^d*New and Renewable Energy Research Division, Korea Institute of Energy Research, Daejeon 305-343, Republic of Korea*

^e*Department of Physics and Astronomy, College of Science, King Saud University, P.O. Box 2455, Riyadh 11451, Saudi Arabia*

^f*World Premier International (WPI) Research Center for Materials Nanoarchitectonics (MANA), National Institute for Materials Science (NIMS), Ibaraki 305-0044, Japan*

[‡] These authors contributed equally to this work.

[§] Present address: School of Energy and Chemical Engineering, Ulsan National Institute of Science and Technology (UNIST), Ulsan 690-798, Republic of Korea

* Corresponding authors: parkms@keti.re.kr; jhk@uow.edu.au

Experimental Section

Synthesis of MnCo₂O₄ and CoMn₂O₄ hollow nanofibres

The MnCo₂O₄ (MCO) and CoMn₂O₄ (CMO) fibres were fabricated by an electrospinning technique. In order to prepare the MCO spinning solution, 0.743 g manganese acetate tetrahydrate (Mn(CH₃COO)₂ · 4H₂O, 99%, Aldrich) and 1.510 g cobalt acetate tetrahydrate (Co(CH₃COO)₂ · 4H₂O, 99%, Aldrich) powders were dissolved in 10 ml N,N-dimethylformamide under gentle magnetic stirring. After about 1 h, 1.3 g poly(vinylpyrrolidone) (PVP, (C₆H₉NO)_n, M_w~1,300,000, Aldrich) was put into the above solution and uniformly mixed for 1 h. For the CMO solution, 0.755 g cobalt acetate tetrahydrate and 1.485 g manganese acetate tetrahydrate powders were used. The transparent solutions were loaded into a plastic syringe equipped with a 23 gauge needle that was electrically connected to a high voltage power supply. The electrospinning of the solutions was carried out under the following ambient conditions: DC voltage of 25 kV, feeding rate of 1.2 ml/h, distance between the needle tip and the Al-foil-wrapped drum collector of 15 cm, and rotation speed of the drum collector of 200 rpm. The electrospun fibres were acquired by detaching them from the collector and subsequently dried at 150 °C for 3 h in a convection oven. Finally, the calcination was performed at 600 °C for 3 h (with a heating rate of 5 °C/min) in ambient air. In order to investigate the effect of the heating rate and calcination temperature on the fibre morphology, the as-dried fibres were subjected to different heat-treatments at 300 °C or to a ramping rate of 0.5 °C/min.

Sample characterisation

The microstructure and morphology of the electrospun fibres were observed by field-emission scanning electron microscopy (FESEM, JSM-7000F, JEOL) and transmission electron microscopy (TEM, JEM-2100F, Japan Electronic Optics). The elemental distributions were examined by TEM- energy dispersive X-ray spectroscopy (EDS) mapping. The phases and crystal structures were identified by using X-ray diffraction (XRD, PAN analytical, Empyrean) with Cu-K α radiation and fast-Fourier transform (FFT) patterns. The porosity was analysed by N₂ sorption isotherms using a surface area and porosimetry analyser (TristarII 3020, Micromeritics). The specific surface area and pore volume were calculated by Brunauer–Emmett–Teller (BET) and Barrett-Joyner-Halenda (BJH) methods, respectively. The thermal behaviour of the as-dried fibres was monitored by thermogravimetric/differential thermal

analyses (TG/DTA, DTG-60H, Shimadzu) with a heating rate of 5 °C/min under air and under flowing Ar gas.

Electrochemical evaluation

The electrochemical properties were evaluated using 2032 coin-type half-cells. The working electrodes were prepared by coating Cu foil with slurries containing the active material (80 wt%), conducting agent (Super-P, 10wt%), and polyacrylic acid binder (PAA, 10wt%) dissolved in deionized water. Afterwards, the electrodes were dried at 80 °C for 10 h in an oven to vaporise the water, pressed under a pressure of 200 kg/cm, and finally dried at 80 °C under vacuum. The electrodes were cut into 12 mm-diameter disks, in which the amount of the active material was around 0.8 mg/cm². The coin cells were carefully assembled in a dry room that provided humidity at a dew point of less than -60 °C. A porous polyethylene film and Li foil (14 mm in diameter) were used as the separator and counter-electrode, respectively. 1 M LiPF₆ dissolved in a mixture of ethylene carbonate (EC) and ethyl methyl carbonate (EMC) in a volume ratio of 1 : 2 was employed as the electrolyte, along with a fluoroethylene carbonate (FEC, 2 wt%) additive. The coin cells were galvanostatically tested with a constant current density of 0.1 C for the first to the third cycle and current density of 0.2 C for subsequent cycles (with 1 C set at 1000 mA/g) within a voltage window of 0.01 to 3.0 V (vs. Li/Li⁺). The charge rate performance was evaluated at various rates from 0.1 C to 5 C, where the discharge rate was fixed at 0.1 C and 0.2 C for charging at 0.1 C and at 0.2 C–5 C, respectively.

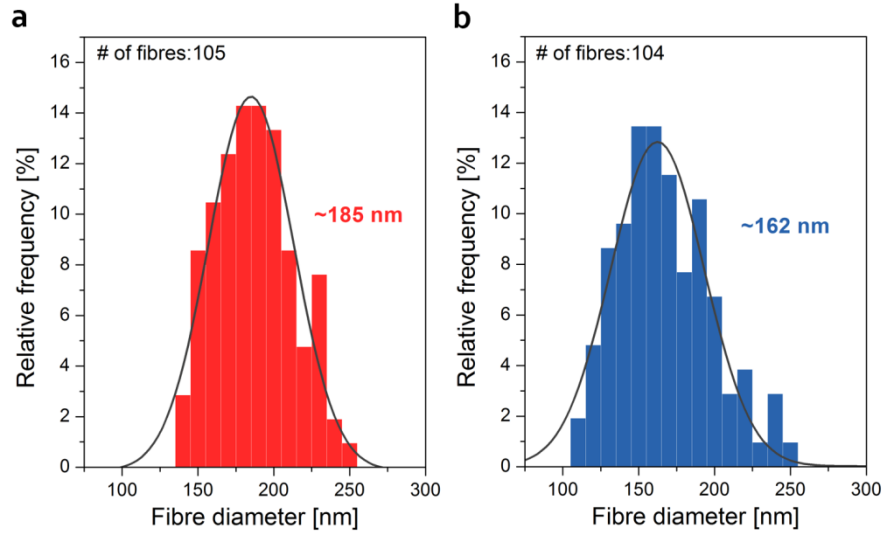


Figure S1. Fibre diameter distributions of (a) MCO and (b) CMO samples after calcination at 600 °C (with a heating rate of 5 °C/min), which were estimated by averaging the diameters of more than 100 fibres in several SEM images.

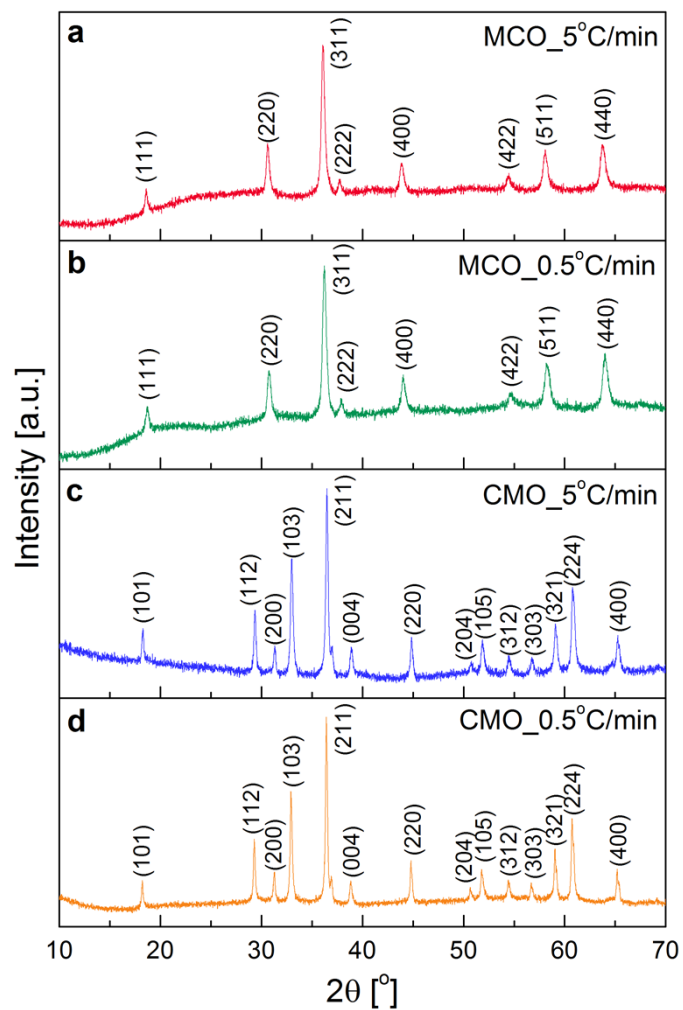


Figure S2. XRD patterns of (a, b) MCO and (c, d) CMO fibres after calcination at 600 °C with a heating rate of 5 °C/min (a, c) and 0.5 °C/min (b, d).

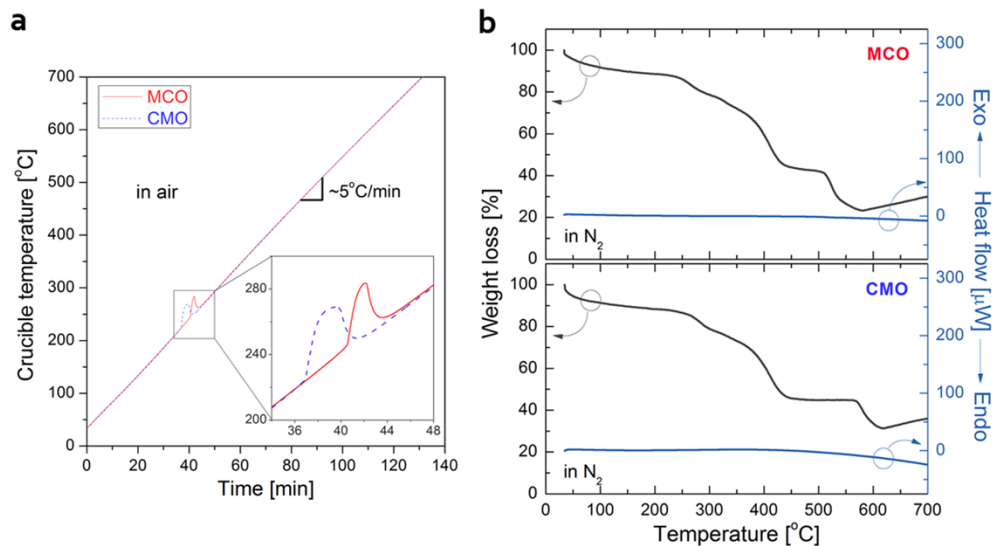


Figure S3. TG/DTA data for as-dried MCO and CMO fibres under (a) air and (b) flowing N₂ atmospheres: (a) crucible temperature as a function of the measurement time during the TG-DTA measurements. The enlarged region marked by the square in (a) shows an abrupt temperature increment in the crucible over the nominal heating rate of 5 °C/min, revealing the occurrence of a highly exothermic reaction during the heat-treatment in air; on the other hand, no notable exothermic peak was found in the DTA curves under N₂ atmosphere for either the MCO or the CMO.

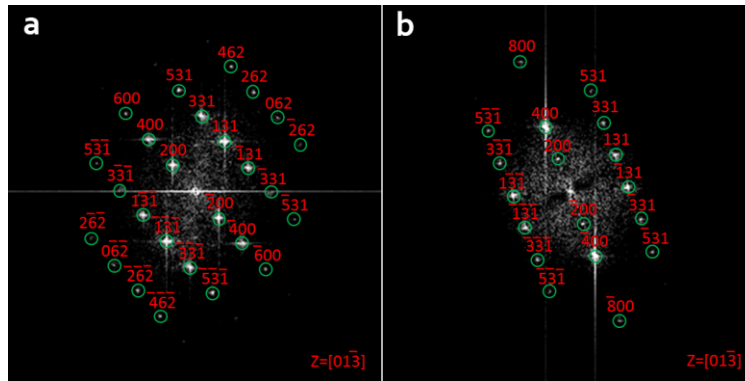


Figure S4. FFT patterns for the inset high-resolution TEM (HRTEM) images in (a) Fig. 3c and (b) Fig. 3d. Both the patterns had the zone axis of $[01\bar{3}]$ for cubic spinel MnCo_2O_4 phase.

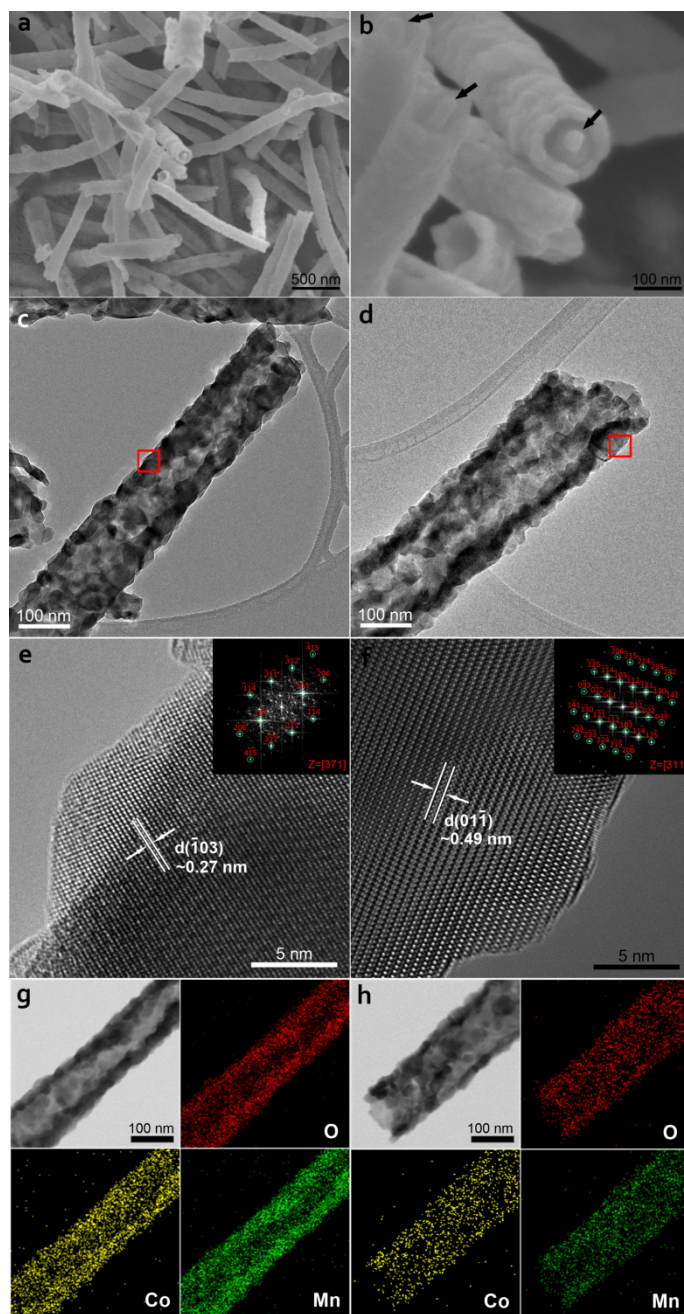


Figure S5. (a, b) SEM, (c-f) TEM, and (g, h) EDS mapping images of CMO fibres annealed at different heating rates of 0.5 °C/min (a, b, c, e, g) and 5 °C/min (d, f, h). The arrows in (b) indicate a core-in-tube morphology; (e) and (f) show HRTEM images of the regions marked by squares in (c) and (d), respectively, and the insets are the corresponding FFT patterns with the zone axes of $[371]$ and $[311]$, respectively; the interplanar spacing in (e) and (f) was measured to be ~ 0.27 nm and ~ 0.49 nm, which were assigned to the $(\bar{1}03)$ and $(01\bar{1})$ planes of the tetragonal spinel CoMn_2O_4 phase, respectively; the EDS data revealed the uniform elemental distributions of O, Mn and Co, and overall, the ratio of Mn to Co was estimated to be ~ 2.1 for both CMO-0.5 and CMO-5.

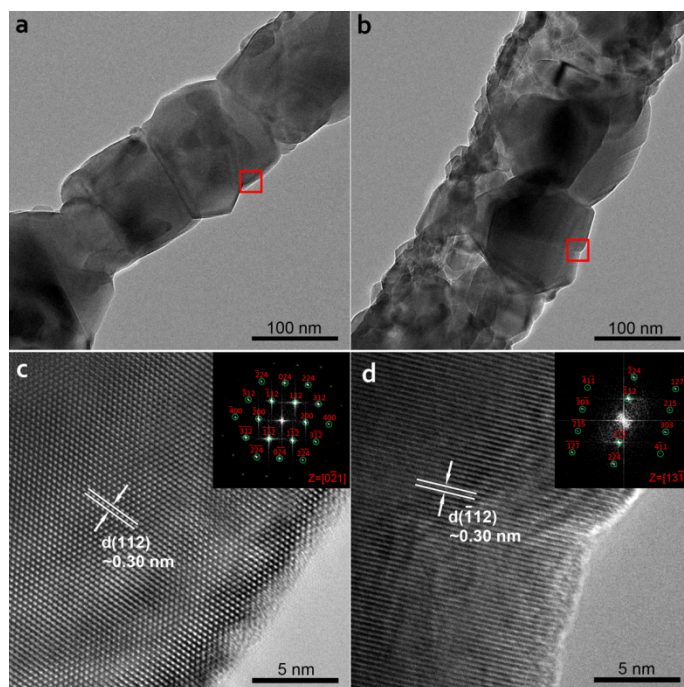


Figure S6. TEM images of the CMO fibres annealed at different heating rates of (a, c) 0.5 °C/min and (b, d) 5 °C/min; (c) and (d) contain the HRTEM images of the regions marked by squares in (a) and (b), respectively, and the insets are the corresponding FFT patterns with the zone axes of $[0\bar{2}1]$ and $[1\bar{3}\bar{1}]$, respectively. The interplanar spacing in (c) and (d) was measured to be ~ 0.30 , corresponding to the (112) and $(\bar{1}\bar{1}2)$ planes of the tetragonal spinel CoMn_2O_4 phase.

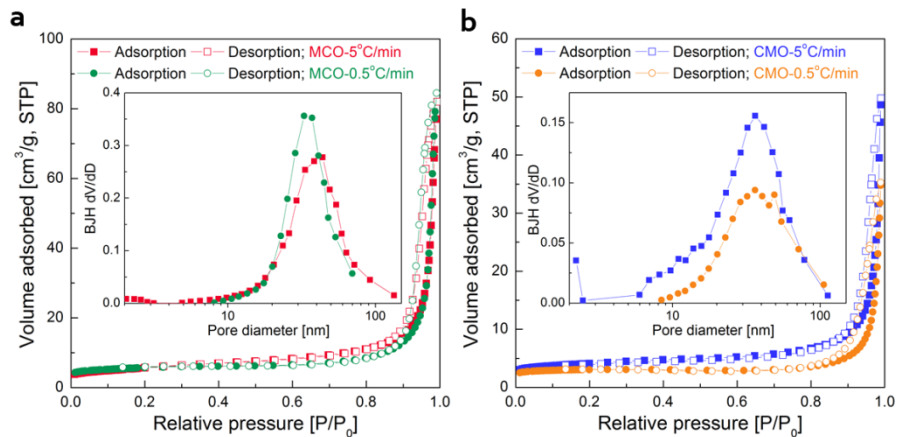


Figure S7. N_2 adsorption/desorption isotherms and pore size distributions calculated by the Barrett-Joyner-Halenda (BJH) method (insets) of (a) MCO and (b) CMO fibres annealed at different heating rates.

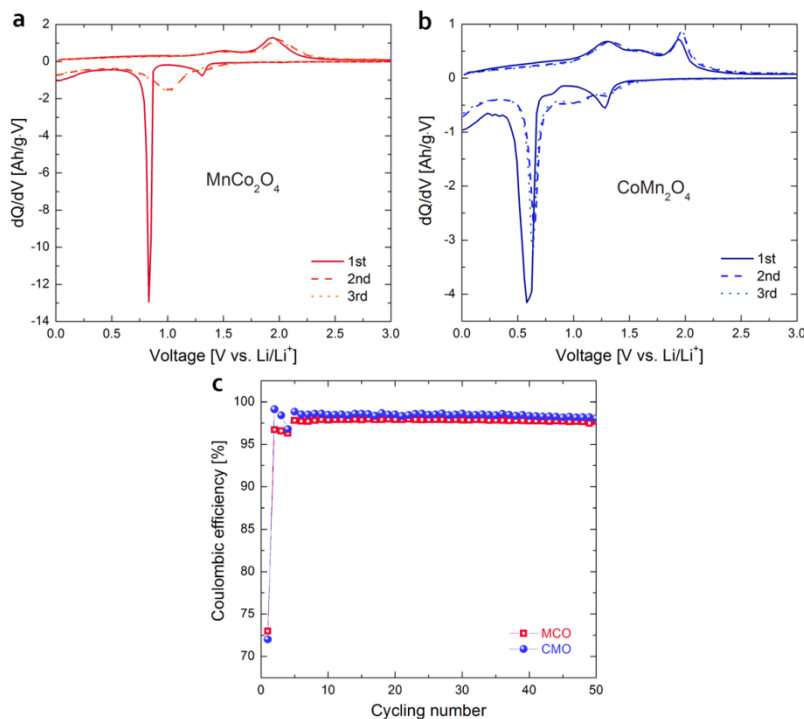
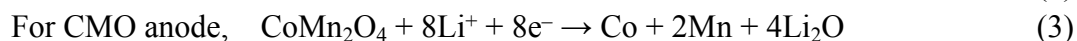
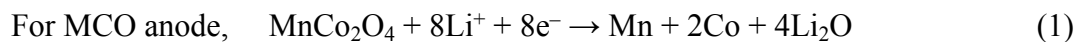


Figure S8. Differential capacity plots (DCPs) of (a, b) galvanostatic voltage profiles for the first 3 cycles, and (c) coulombic efficiency over 50 cycles of MCO-5 and CMO-5 fibre anodes.

The DCP of the first cycle is obviously different from those of the subsequent cycles for both the MCO and the CMO anodes. In the case of the MCO anode (Fig. S8a), a small cathodic peak at ~ 1.3 V in the first cycle can be assigned to the reduction of Co^{3+} to Co^{2+} and the following sharp, large peak at ~ 0.83 V is attributed to the reduction of both Co^{2+} and Mn^{2+} to metallic Co and Mn. In the anodic region, two broad peaks at ~ 1.5 V and ~ 1.9 V are found, corresponding to the oxidation of Mn to Mn^{2+} and Co to Co^{2+} , respectively. In the second and third cycles, a broad reduction peak at ~ 1.0 V is observed. For the CMO sample (Fig. S8b), two notable reduction peaks at ~ 1.28 V and ~ 0.58 V are seen in the cathodic region of the first cycle, which are related to the reduction of Mn^{3+} to Mn^{2+} and the further reduction of Mn^{2+} to Mn and Co^{2+} to Co, respectively. A small reduction peak at ~ 0.8 V is probably attributable to the SEI formation. In the following anodic process, two broad peaks are found at ~ 1.3 V and ~ 1.9 V, due to the oxidation of Mn and Co, respectively. In the subsequent cycles, the repeated reduction/oxidation reactions occur in two pairs of redox peaks at $\sim 0.64/\sim 1.3$ V and $\sim 1.0/\sim 2.0$ V for MnO and CoO, respectively. Based on the above reactions, the overall electrochemical process can be described as follows:



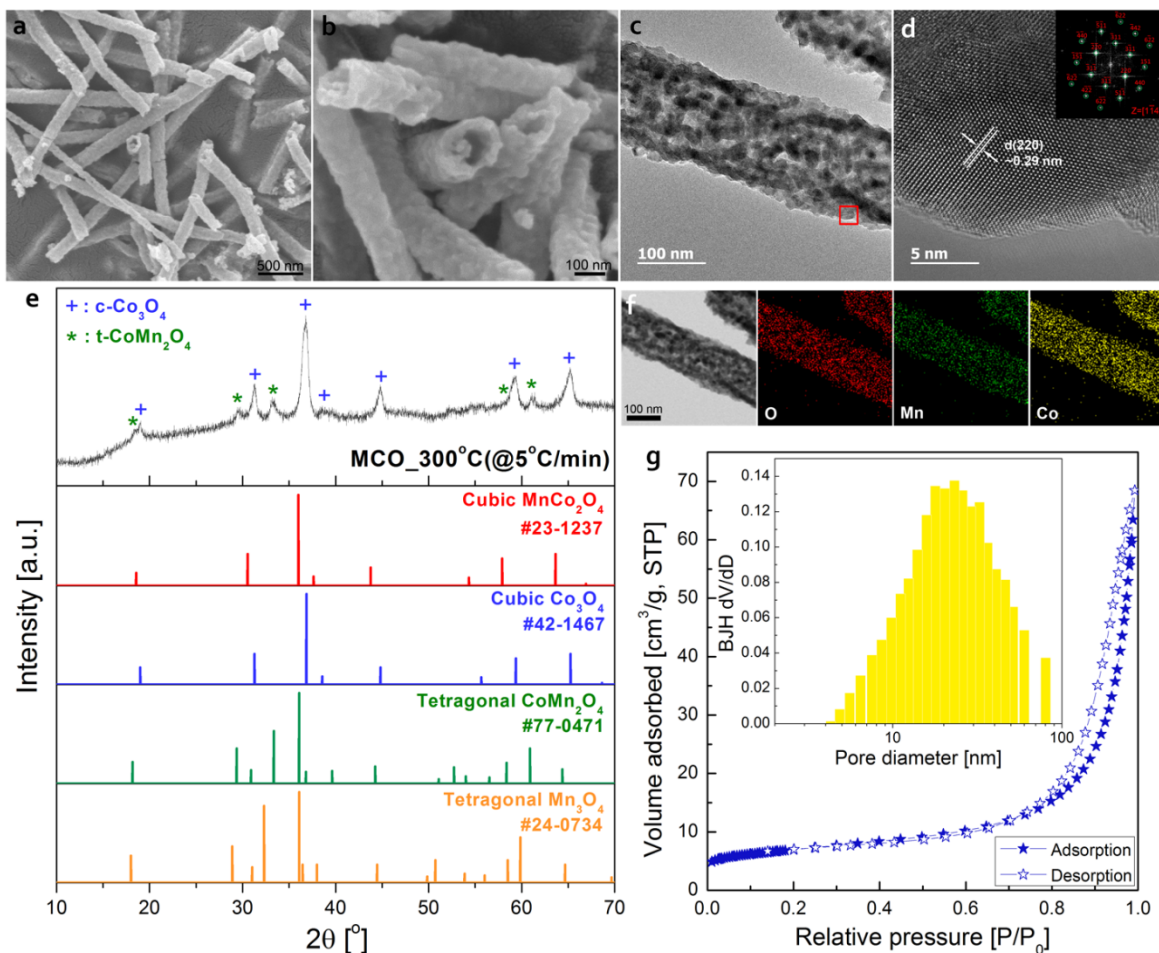


Figure S9. (a, b) SEM, (c, d) TEM, (e) XRD, (f) TEM-EDS mapping, and (g) N_2 adsorption/desorption isotherm data for MCO fibres heat-treated at 300 °C with a ramping rate of 5 °C/min; (d) contains an HRTEM image of the region marked by the square in (c), and the inset is the FFT pattern with the zone axis of $[1\bar{1}4]$; the interplanar spacing was measured to be ~ 0.29 nm, corresponding to the (220) plane of cubic Co_3O_4 phase (space group $Fd\bar{3}m$ (227), JCPDS No. 42-1467); the bottom panels in (e) contain the reference XRD patterns; the inset in (g) displays the pore size distribution calculated by the BJH method; D_{pore} , V_{pore} , and S_{BET} were estimated to be 15.2 nm, 0.092 cm^3/g , and 24.1 m^2/g , respectively.